

Physico-Chemical and Morphological Characterization of Cellulosic Samples Obtained from Sisal Fibers

G. Mondragon, C. Peña-Rodriguez, A. Eceiza and A. Arbelaz*

'Materials + Technologies' Group, Chemical and Environmental Engineering Department, Faculty of Engineering, Gipuzkoa, University of the Basque Country UPV/EHU, Pza. Europa 1. 20018, Donostia-San Sebastián, Spain

Received September 22, 2016; Accepted January 24, 2017

ABSTRACT: In this work, the main chemical reactions conditions of a succession of specific chemical treatments used for the isolation of nanocellulose from sisal fibers were evaluated. The novelty of this work is the study done to analyze the effect of different reaction conditions (time or concentration) in fiber structure and composition as well as in the characteristics of obtained cellulosic samples. In order to achieve this goal different physicochemical, thermal and morphological characterization techniques were used after each chemical treatment and the most suitable reaction conditions were selected for the subsequent treatment. Moreover, the thermal stability evolution of cellulose nanocrystals during the dialysis process was evaluated.

KEYWORDS: Sisal fiber, chemical treatments, nanocellulose, thermal stability

1 INTRODUCTION

Raw materials obtained from renewable sources such as lignocellulosic fibers have attracted considerable attention because they could be good candidates to develop more sustainable materials [1]. Lignocellulosic fibers are mainly composed of cellulose, hemicellulose and lignin [2, 3] and these fibers are used as reinforcements in polymeric matrix composites [4–6]. Lignocellulosic fibers can also be used as a source of nanocellulose due to their high cellulose and low lignin content [7, 8]. As detailed in a previous work [9], cellulosic samples and nanocellulose can be isolated using a succession of specific chemical treatments, being alkali treatment, acetylation and acid hydrolysis the main reactions that produce the main changes in fiber structure. First, cellulose nanofibers (CNFs), which are formed by crystalline and amorphous domains, were obtained, and thereafter, by acid hydrolysis, cellulose nanocrystals (CNCs). These CNCs have a modulus value close to the perfect crystal of native cellulose (~ 150 GPa) and high aspect ratio values [10, 11]. There are many works in the literature in which nanocelluloses, due to their outstanding specific properties, have been used as reinforcement in polymeric matrix nanocomposites [12, 13]. However, the thermal degradation of cellulose

limits the use of CNC in nanocomposites prepared by melt blending of thermoplastic polymeric matrices. The processing temperature of many thermoplastic polymers is superior to 200 °C, so that the thermostability of CNC is important for nanocomposite fabrication. The CNCs isolated by acid hydrolysis with sulfuric acid have sulphate groups on the surface, leading to the low thermal stability of cellulose [14, 15]. An alternative to enhance the thermal stability of CNCs can be the isolation of them by the use of hydrochloric acid. However, the isolated CNCs tend to aggregate due to the absence of surface charge on crystals [16].

In this work, the main chemical treatments used for the isolation of nanocellulose were evaluated. This work aims to characterize physico-chemically and morphologically the cellulosic samples obtained from sisal fibers using different chemical reaction conditions. The novelty of this work is the study done to analyze the effect of different reaction conditions (time or concentration) in fiber structure and composition as well as in the characteristics of obtained cellulosic samples. Moreover, the thermal stability evolution of CNCs during the dialysis process was evaluated. Characterization was done by means of Fourier transform infrared spectroscopy (FTIR), X-ray diffraction (XRD), thermogravimetric analysis (TGA) and optical (OM) and atomic force microscopy (AFM) techniques.

*Corresponding author: aitor.arbelaz@ehu.eus

DOI: 10.7569/JRM.2017.634124

2 MATERIAL AND METHODS

Sisal fibers (S) used in this work were provided by Celulosa de Levante, S.A., Spain. The chemicals employed for the specific chemical treatments were sodium hydroxide pellets PA-ACS-ISO, glacial acetic acid QP, nitric acid PA-ISO (65% purity) and sulphuric acid PA-ISO (96% purity) supplied by Panreac. All chemicals were used as received without further purification.

As detailed in a previous work [9], nanocelluloses can be isolated from sisal fibers using a succession of specific chemical treatments based on extractives (E), prealkalization (PA), alkalization (A), acetylation (Ac) and acid hydrolysis (H) treatments. Among them, alkali, acetylation and acid hydrolysis treatment conditions were evaluated in this work because they produce the main changes in fiber structure and composition. In the extractives treatment, which is based on the standard method of TAPPI T204 cm-97, waxes and oils are removed. During prealkalization treatment, fibers are swollen and part of the hemicelluloses and lignins are removed. Thereafter, the alkali treatment removes more hemicelluloses and lignins and individualizes each elementary fiber. The goal of acetylation treatment is to remove residual cementing material to obtain cellulose nanofibers (CNFs). In a previous work [9], it was observed that acetylation process of stirred sample was effective to obtain CNF composed by crystalline and amorphous regions. However, the severity of the treatment used is not enough to remove amorphous zones, therefore, a solution of concentrated sulphuric acid was used to remove amorphous cellulose and isolate cellulose nanocrystals (CNCs).

To remove the extractives, such as waxes and oils (E), fibers were immersed in a solvent mixture of ethanol/toluene 1:2 (v/v). In order to swell the fibers, fibers without extractives were treated with 2 wt% NaOH solution (PA) for 12 h at 40 °C. After that, to remove more amount of hemicelluloses and lignins, fibers were subjected to an alkali treatment (A) with 7.5 wt% NaOH solution and different reaction times of 60, 90, 120 and 240 minutes were evaluated. These alkali-treated samples were denoted as A60, A90, A120 and A240, respectively. After washing alkali-treated samples with deionized water until pH 6, to extract CNF, fibers were acetylated with an acid solution of acetic and nitric acids (6:1 v/v) for different reaction times of 30, 60 and 90 minutes. The fiber/solution ratio used was 0.6:14 (w/v) and these samples were denoted as Ac30, Ac60 and Ac90. Samples were washed with deionized water until pH 6. Finally, in order to isolate CNC, acetylated nanofibers were treated with different sulphuric acid concentrations (32 and 64 wt%) at 45 °C for different chemical reaction

times (30, 60 and 120 minutes) under continuous stirring. Afterwards, the reaction was stopped by adding water and the suspension was washed with deionized water using repeated centrifugation cycles until the supernatant became turbid. The solid part was dialyzed with deionized water for 4–5 days until different pH values were reached. Spectra/Por® 2 standard grade regenerated cellulose membranes with a molecular weight cut off of 12000–14000 Dalton were used for the dialysis process. Hydrolyzed samples were denoted as H32-60 and H32-120 when samples were treated with 32 wt% sulphuric acid concentration for 60 and 120 minutes, respectively. When samples were treated with 64 wt% sulphuric acid concentration for 30 and 60 minutes, they were denoted as H64-30 and H64-60, respectively.

Fourier transform infrared spectra were recorded on a Nicolet Nexus 670 FTIR spectrometer in the range of 4000–400 cm⁻¹ using KBr. Spectra were taken with a resolution of 2 cm⁻¹ with a total of 40 scans for each sample.

X-ray diffraction patterns of each sample were collected using a PHILIPS X'PERT PRO automatic diffractometer operating at 40 kV and 40 mA, in theta-theta configuration, secondary monochromator with Cu-K α radiation ($\lambda = 1.5418\text{\AA}$) and a PIXcel solid-state detector. Data were collected at 2θ from 6 to 60°. The crystallinity index (CI) of cellulose samples has been calculated from the diffracted peak intensity data using the method of Segal *et al.* (Equation 1) [17]:

$$CI = \left(\frac{I_{002} - I_{am}}{I_{002}} \right) 100 \quad (1)$$

where I_{002} was the maximum intensity of the (002) lattice diffraction peak (diffraction angle at around 2θ of 23°) and I_{am} was the intensity corresponding to diffraction angle at around 2θ of 18°.

Thermogravimetric analysis was performed to compare the thermal stability of cellulosic samples. Dynamic thermogravimetric measurements were performed by using a TGA/SDTA 851 Mettler Toledo instrument. Tests were run from 25 to 800 °C at a heating rate of 10 °C/min. These tests were carried out under nitrogen atmosphere (10 mL/min) in order to prevent any thermoxidative degradation. The onset temperature (T_{onset}), determined by a crosspoint given by the tangents where the change in slope of the curve is given, and the maximum degradation temperatures (T_{max}) were collected.

The morphology of cellulosic samples was observed using a Nikon Eclipse E600 optical microscopy. In order to examine the dimensions of cellulose nanoentities, an atomic force microscope (AFM) from Digital Instruments having a NanoScope III controller with

a MultiMode head (Veeco) with an integrated silicon tip/cantilever was used. AFM height images were obtained operating in tapping mode and the diameters of CNCs were calculated from the height profiles.

3 RESULTS AND DISCUSSION

3.1 The Effect of Alkali Reaction Time on Properties of Cellulosic Samples

Figure 1a–c shows FTIR spectra, X-ray diffractograms, TG thermograms and their derivative curves (DTG) of cellulosic samples obtained after different alkali reaction times. The changes in infrared absorption bands (Figure 1a) indicate that the composition of the fibers varied after alkali treatment. For comparison purposes, the spectra of untreated and prealkali treated fibers are shown. The peak at 1740 cm^{-1} in untreated sisal fibers attributed to C=O stretching of the acetyl and ester groups in hemicelluloses and in aromatic components

of lignin [18, 19] was not observed in alkali samples. The absorption band at 1595 cm^{-1} associated with C=C in plane symmetrical stretching vibration of aromatic ring present in lignin [20, 21] decreased slightly when the alkali reaction time was increased. On the other hand, the intensity of the absorption band at 1057 cm^{-1} attributed to C–O–C stretching of the pyranose ring skeletal vibration of cellulose [22, 23] was increased with reaction time, indicating that cellulose content in the fibers increased after alkali treatment.

Figure 1b shows X-ray diffractograms of untreated sisal fibers and alkali-treated samples for different reaction times. The intensity of peaks around $2\theta = 15.0^\circ$, 16.7° , 23.0° and 34.8° attributed to cellulose I structure [24] increased after alkali treatment. The peaks present at $2\theta = 15.0^\circ$ and 16.7° became more pronounced when the cellulose content in fibers increased [25]. The relative crystallinity index (CI) of samples was calculated from X-ray diffraction patterns and the values are reported in Table 1. The crystallinity

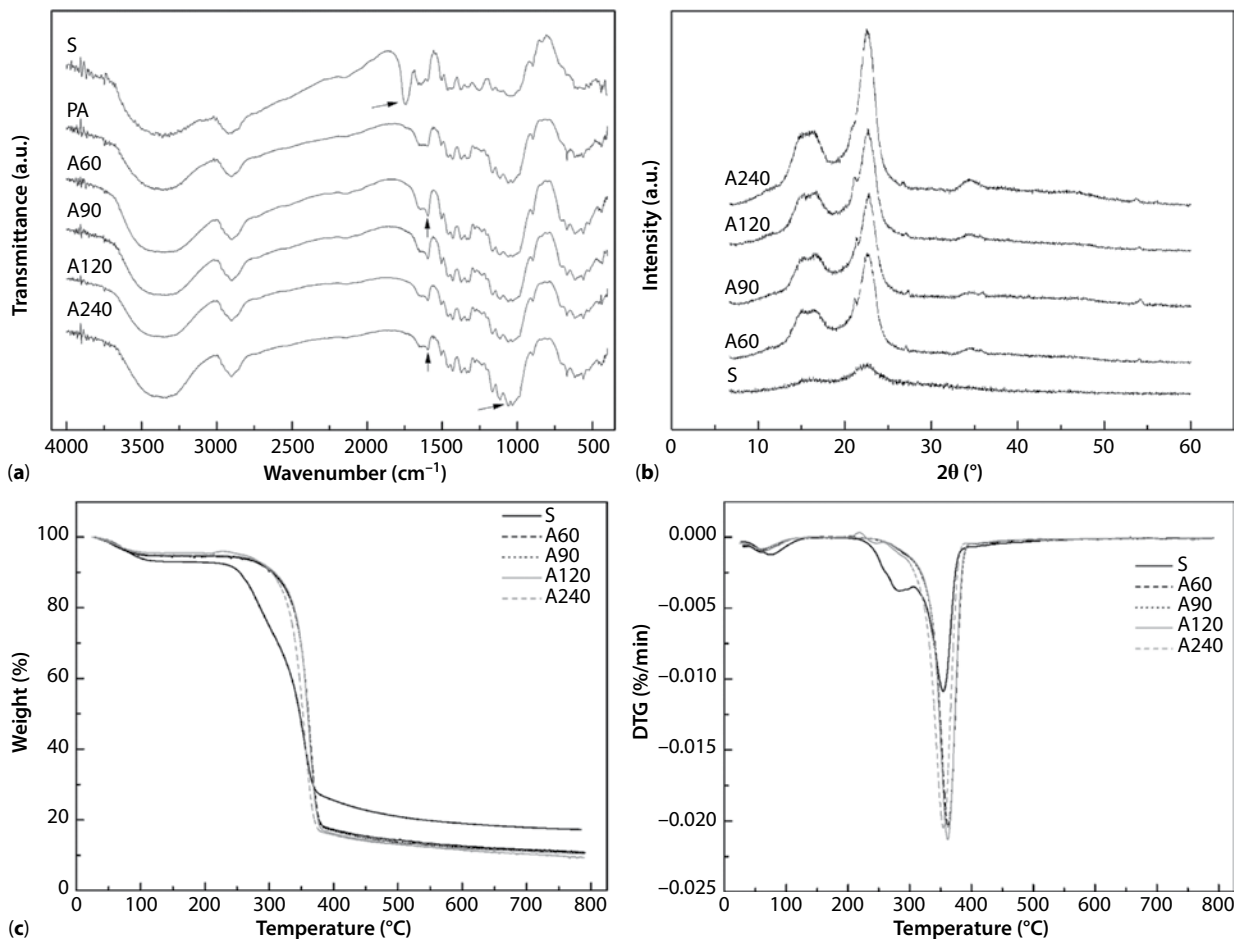


Figure 1 The effect of different alkali reaction times on the obtained cellulosic samples: (a) FTIR spectra, (b) XRD diffractograms and (c) TG and DTG curves.

index values of alkali-treated fibers were higher than untreated sisal fibers. Barreto *et al.* [26] reported CI values of 69 and 66% for sisal fibers treated with 5 and 10 wt% NaOH solutions, respectively. Similar CI values were obtained for alkali-treated samples, obtaining the highest CI value when the reaction time was 240 minutes. This result is in accordance with the intensity increment in the band at 1057 cm^{-1} associated with cellulose observed in the FTIR spectra.

The TG thermograms and their derivative curves (DTG) of alkali-treated sisal fibers after different reaction times are shown in Figure 1c. The first stage of weight loss, the onset and the maximum degradation temperatures and residue content at $800\text{ }^{\circ}\text{C}$ are reported in Table 2. Alkali-treated fibers showed an initial weight loss related to the evaporation of absorbed water. After the alkali treatment, the thermal stability of fibers was improved because hemicelluloses which degraded at lower temperature were removed [27].

Table 1 Crystallinity index values of alkalization, acetylation and acid hydrolysis chemical reactions.

Treatment	Treatment time (min)	CI (%)
S	0	47
A60	60	62
A90	90	63
A120	120	65
A240	240	70
Ac30	30	76
Ac60	60	78
Ac90	90	75
H32-60	60	77
H32-120	120	67
H64-30	30	79
H64-60	60	72

However, after samples were alkali treated for 240 minutes, fibers showed a reduction in the onset and maximum degradation temperature values.

Figure 2 shows optical images of untreated sisal fibers, prealkali treated and alkali-treated samples during different reaction times. Untreated and prealkali treated samples showed fiber bundles which were composed by many unitary fibers cemented together by noncellulosic materials (lignin, hemicellulose, pectin). After alkali treatment with 7.5 wt% NaOH solution, fiber bundles started to defibrillate due to the removal of cementing materials and unitary fibers with diameters of about $10\text{ }\mu\text{m}$ can be observed. Rosli *et al.* [25] also observed that sisal fibers started to defibrillate after an alkali treatment. Among alkali-treated fibers using different reaction times, there were no significant differences in surface morphology.

Taking into account the results obtained from different characterization techniques, the alkali treatment for 240 minutes was discarded due to the reduction observed in onset and maximum degradation temperatures. The results for the rest of the alkali reaction times were very similar. Cellulosic fibers obtained using the intermediate alkali reaction time of 90 minutes was selected for the next acetylation treatments.

3.2 The Effect of Acetylation Reaction Time on Properties of Cellulosic Samples

Figure 3a shows FTIR spectra of cellulosic samples after acetylation treatment for different reaction times. The bands observed in acetylated samples around 1735 cm^{-1} , attributed to C=O stretching vibration of acetyl group, and around 1248 cm^{-1} , attributed to -C-O- stretching of acetyl groups, confirmed that acetylation had taken place [22, 28, 29]. The absorption bands at 1595 cm^{-1} and 1504 cm^{-1} observed in alkali-treated sample spectra, related to the aromatic skeletal vibration present in lignin [21, 23, 30], disappeared

Table 2 The TG experimental values of raw fibers and after some studies of different chemical reactions.

Treatment	1st stage weight loss	2nd stage T_{onset}	Degradation T_{max}	Residue at $800\text{ }^{\circ}\text{C}$
	(%)	($^{\circ}\text{C}$)	($^{\circ}\text{C}$)	(%)
S	7	253	354	17
A60	6	338	362	11
A90	6	338	362	11
A120	5	340	361	9
A240	4	327	354	10
Ac30	4	327	350	11
Ac60	3	319	350	11
Ac90	5	312	331	11

in all acetylated samples, suggesting that lignin was removed after acetylation treatment. Moreover, after acetylation treatment, the band at 1057 cm^{-1} related to β -glycosidic linkage between glucose units in cellulose became more distinguishable than in alkali-treated sample.

Figure 3b shows X-ray diffraction patterns of acetylated fibers for different reaction times. All acetylated samples showed the cellulose I structure. After acetylation treatment, the main peaks of cellulose were more pronounced due to the removal of lignin, which is in agreement with FTIR results. The crystallinity index (CI) values of acetylated fibers are summarized in Table 1. Acetylated samples showed higher CI values than alkali-treated ones due to the removal of non-cellulosic components.

Figure 3c shows TG thermograms of acetylated samples. It was observed that as the reaction time was increased the onset temperature decreased. As shown in Table 2, acetylated fibers for 30 and 60 minutes showed the highest maximum degradation temperature with a value of $350\text{ }^{\circ}\text{C}$. By contrast, when fibers were acetylated for 90 minutes, this value decreased until $331\text{ }^{\circ}\text{C}$. This fact could be associated with the higher damage in the fibers' structure.

Figure 4 shows OM and AFM height images of acetylated fibers for different reaction times. The AFM

images revealed that CNFs were obtained after acetylation treatments. The AFM height images showed some fine and large cellulose nanofibers which were 5–10 nm in diameter and several micrometers in length. Acetylation reaction caused a reduction in the number of intermolecular hydrogen bonds and some CNFs can be obtained just by stirring the sample suspension, as can be observed by AFM. Moreover, as can be observed in optical images, fibers barely maintained their structure after acetylation treatments. Taking into account the onset temperature value, acetylated fibers for 30 minutes were selected for further hydrolysis reactions.

3.3 The Effect of Acid Hydrolysis Reaction Conditions on Properties of CNC Samples

Figure 5a–c shows FTIR spectra, X-ray diffractograms, TG thermograms and their derivative curves (DTG) of cellulosic samples obtained after different acid hydrolysis treatments. The FTIR spectra of samples after acid hydrolysis treatments under different times and concentrations are shown in Figure 5a. The band around 1735 cm^{-1} attributed to the acetyl group can still be observed in all samples. It was supposed that

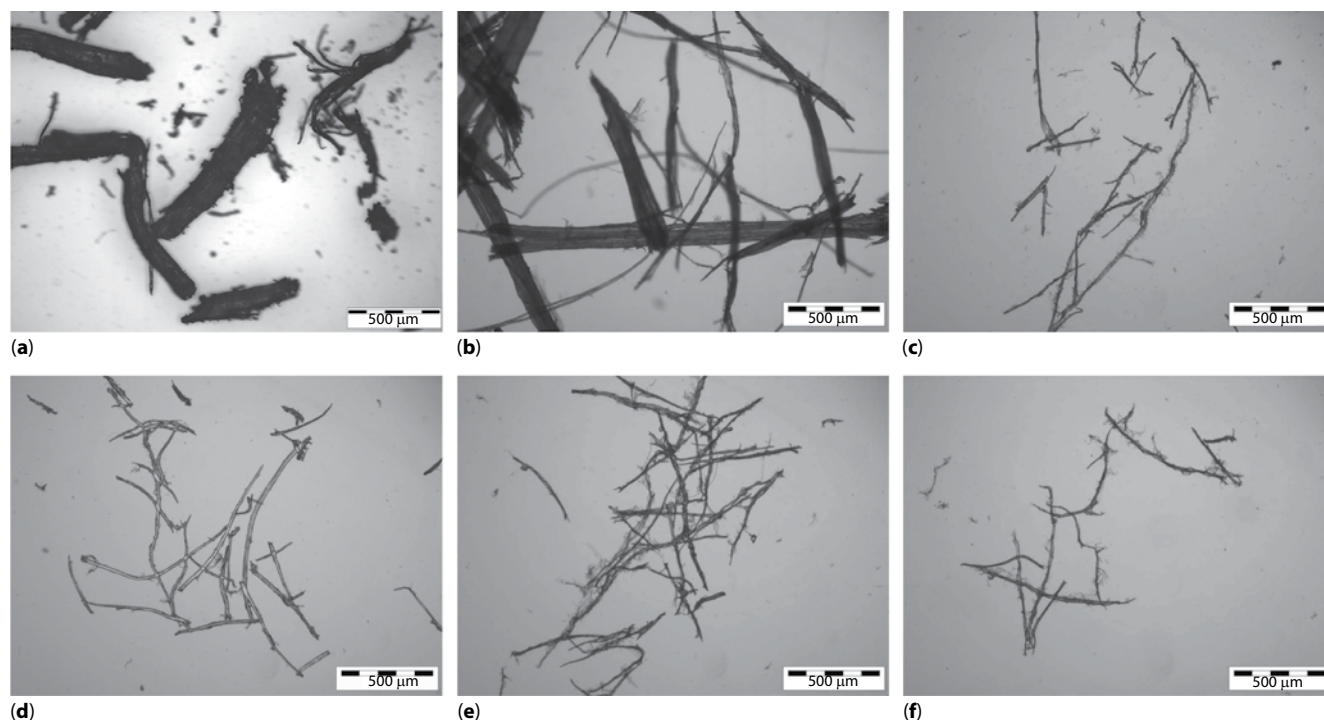


Figure 2 Optical images detailing the morphology of raw sisal fibers, prealkali treated fibers (PA) and alkali-treated sisal fibers (A) in different chemical reaction times: (a) raw fibers, (b) PA, (c) A60, (d) A90, (e) A120 and (f) A240.

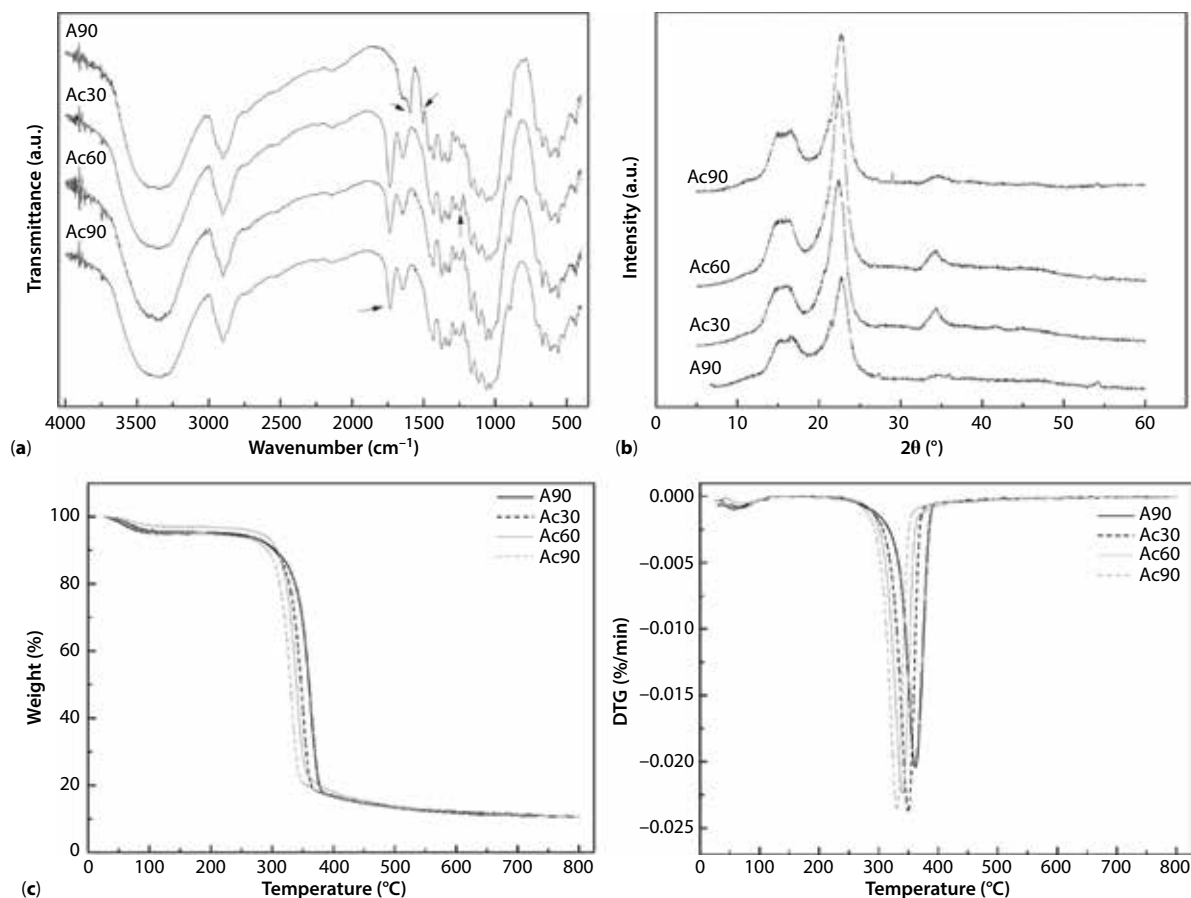


Figure 3 The effect of different acetylation reaction times on the obtained cellulosic samples: (a) FTIR spectra, (b) XRD diffractograms and (c) TG and DTG curves.

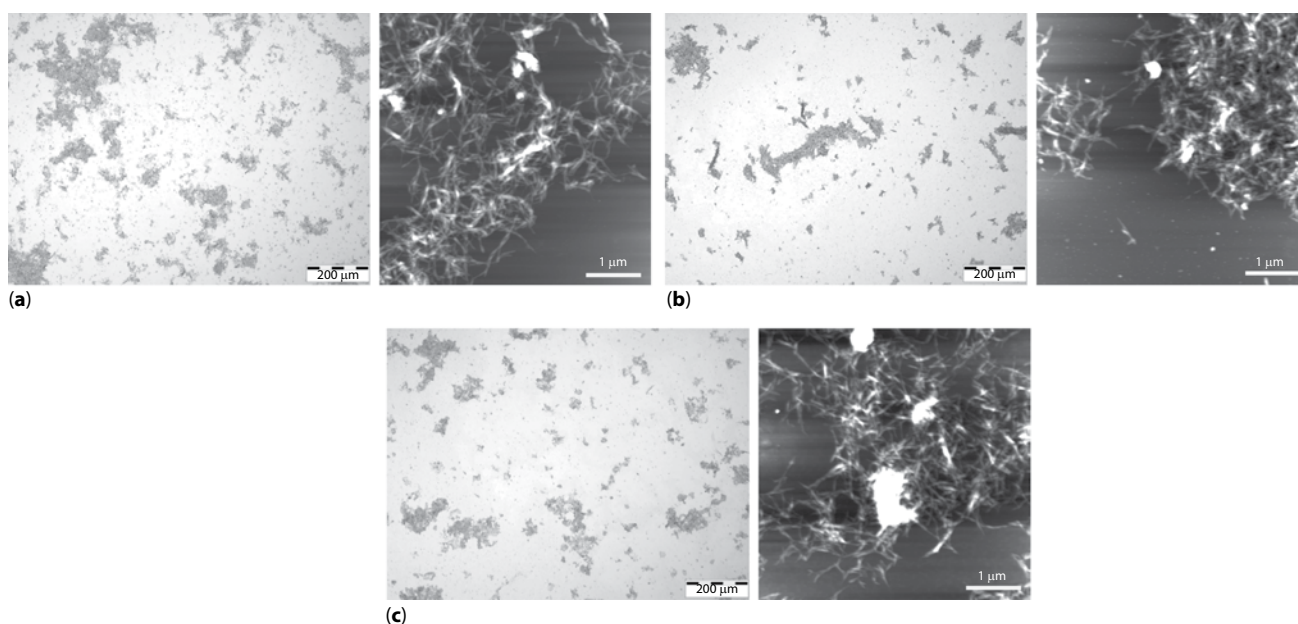


Figure 4 Optical (left) and AFM height (right) images detailing the morphology of acetylated sisal fibers (Ac) in different chemical reaction times: (a) 30 min, (b) 60 min and (c) 90 min.

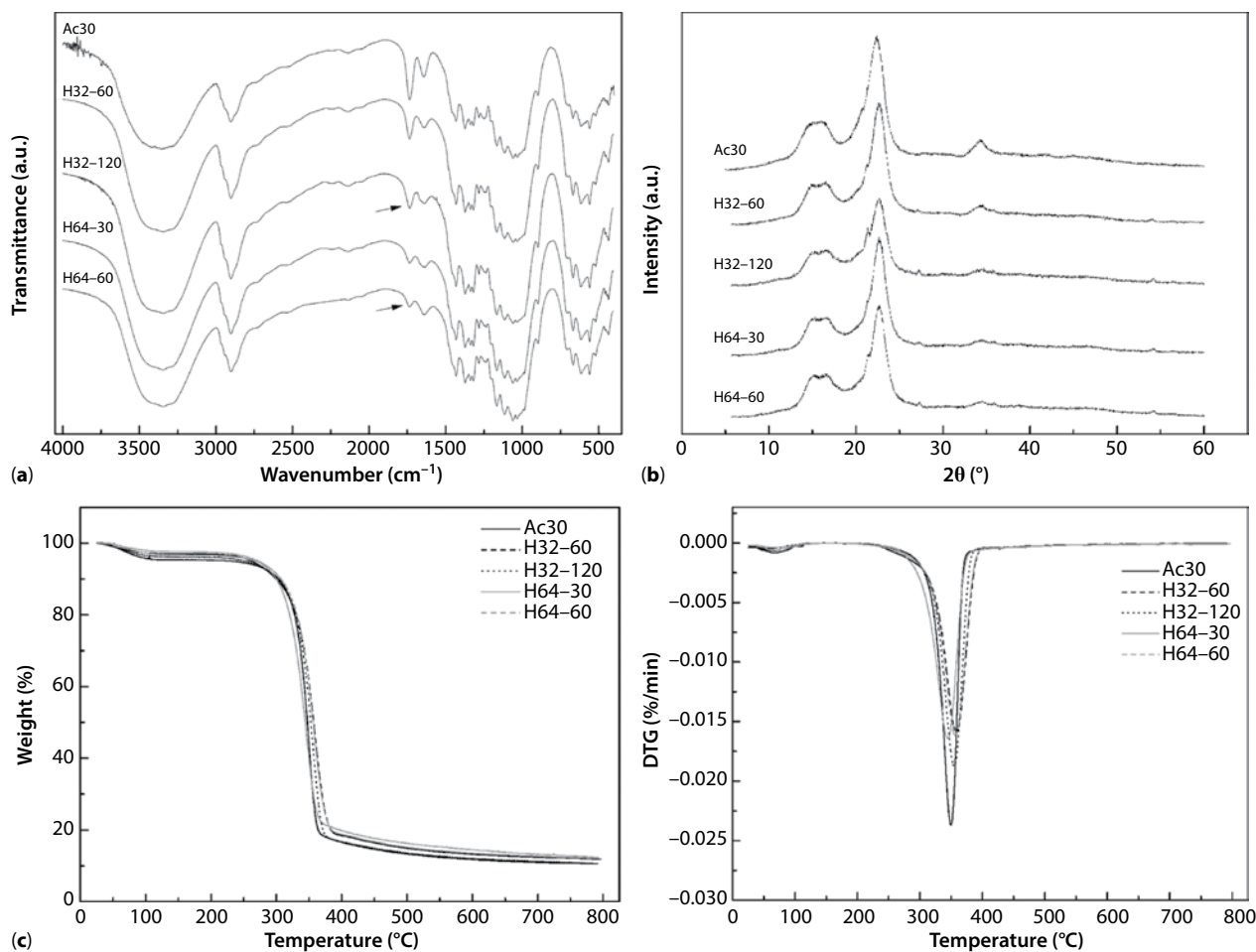


Figure 5 The effect of different acid hydrolysis reaction conditions on CNC samples: (a) FTIR spectra, (b) XRD diffractograms and (c) TG and DTG curves at pH ~ 5.5.

acetylation reaction was mainly carried out in amorphous cellulose due to the hydroxyl groups being more accessible. The decrease in intensity of this band was considerably more when the acid concentration used was higher. This fact could suggest a major elimination of the amorphous part.

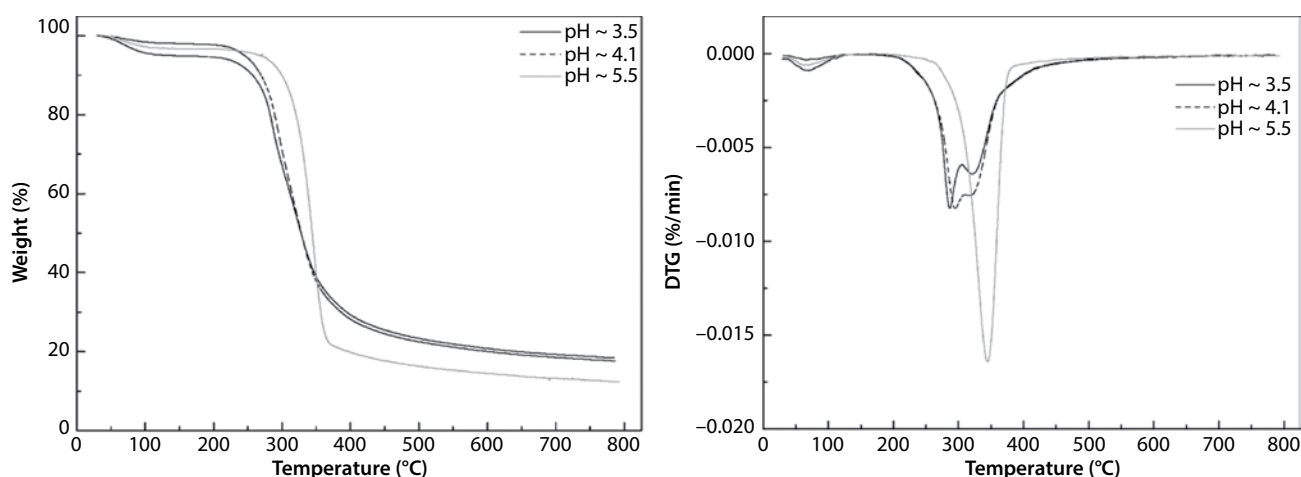
Figure 5b displays X-ray diffraction patterns of acid-hydrolyzed samples and their crystallinity index (CI) values are summarized in Table 1. After acid hydrolysis treatments, cellulose I structure was maintained and CI values obtained were similar to acetylated sample ones. Acid hydrolysis treatment, in addition to dissolving the amorphous region of cellulose [16, 31, 32], could attack the crystalline regions [33]. As reported in Table 1, samples hydrolyzed with 32 wt% of sulphuric acid for 60 minutes and 64 wt% of sulphuric acid for 30 minutes showed the highest CI values, being quite similar in both conditions. However, as seen in Table 1, when hydrolysis times increased, CI values decreased in both concentrations, suggesting

that prolonged hydrolysis might produce some damage in crystal structures. Kargarzadeh *et al.* [33] isolated cellulose nanocrystals from kenaf bast fibers using the following sequence of chemical treatments: alkali treatment, bleaching treatment and subsequent hydrolysis with sulphuric acid. They studied the influence of hydrolysis reaction time on sample crystallinity using X-ray diffraction technique. They observed that even though the crystallinity of samples increased after sulphuric acid hydrolysis reaction, long hydrolysis reaction times reduced the crystallinity of samples due to the destruction of the crystals.

Figure 5c shows TG thermograms and their derivative curves (DTG) of CNC samples dialyzed until pH 5.5. The results obtained after using different hydrolysis conditions were similar. The thermal stability of CNC samples changed during the dialysis process (Table 3). In all samples, the thermal stability of CNC was improved, increasing suspension pH value. According to Mandal and Chakrabarty [29], the thermal

Table 3 The evolution of CNC thermal characteristics in function of different experimental conditions of acid hydrolysis and pH values of the dialyzed CNC suspension.

Treatment	Dialyzed suspension pH	1 st stage weight loss	2 nd stage T _{onset}	Degradation T _{max}	Residue at 800 °C
		(%)	(°C)	(°C)	(%)
H32-60	3.9	3	303	335	13
	5.5	3	326	358	12
H32-120	3.8	3	304	335	11
	5.5	4	327	355	11
H64-30	3.5	5	266	287 and 321	18
	4.1	2	268	295 and 317	18
	5.5	3	315	345	12
H64-60	4.0	4	309	337	13
	5.5	2	328	357	12

**Figure 6** The influence of pH value in CNC thermal degradation behavior for 64 wt% solution in 30 minutes (H64-30): TG and DTG curves.

stability of the CNCs was reduced by the introduction of sulphate groups into the crystals of cellulose in acid medium. Acid medium could catalyze the cleavage of β -1,4-glycosidic bonds between two anhydroglucose units [34, 35] and this cellulose chain length reduction could be the reason for lower thermal stability. Except for CNC obtained after 64 wt% sulphuric acid solution for 30 minutes, all samples showed one degradation step. Figure 6 shows the influence of pH suspension on CNC thermal stability for samples obtained with 64 wt% sulphuric acid solution after 30 minutes. As can be seen, at low pH values, two separated pyrolysis processes were observed. As pH value increased, the onset degradation temperature increased; moreover, in pH around 5.5 a unique degradation step occurred. When two separated degradation processes were observed the residue quantity at 800 °C was

considerably higher than when only one degradation process was observed. This fact can be related to the sulphate content of samples [16, 36]. From Table 3 it was concluded that the sample obtained after 64 wt% sulphuric acid solution for 30 minutes and dialyzed until pH value of 3.5 showed the lowest thermal stability. Moreover, this sample showed the highest residue quantity at 800 °C, suggesting that this one seemed to have the highest sulphate group content. An attempt was made to determine cellulose nanocrystals sulphur content values during the dialysis process by elemental analysis. However, these values were not possible to determine because they were below the control threshold, lower than 3%. The acid concentration was adjusted in a similar way for samples hydrolyzed during 30 minutes and 60 minutes, respectively. As samples were not dried before the hydrolysis step, to avoid

agglomeration of CNFs an average value of suspension solid content which was determined experimentally was used as reference to get the necessary grams of CNF for hydrolysis reaction. However, the actual real grams could be slightly different than the theoretically calculated ones. Taking into account the char contents, it seemed that the sulphuric acid-to-cellulose ratio might be higher for sample hydrolyzed with 64 wt% sulphuric acid solution for 30 minutes than sample hydrolyzed for 60 minutes. Previous to the thermogravimetric analysis, samples were dried and, consequently, covalently linked and free sulphuric acid molecules might be distributed along the sample surface. The sulphuric acid is considered as dehydration catalyst [36]. A possible reason for the two separated degradation processes could be due to zones rich in sulphuric acid molecules and zones poor in sulphuric acid molecules. The first degradation peak observed might be related to zones rich in sulphuric acid molecules. As pH of suspension was increased the first degradation peak temperature value increased. When the pH of suspension was increased until 5.5, the char residue value decreased until 12%, suggesting that sulphate content was decreased in the suspension. The reduction of char content in the sample seemed to be related to the removal of free acid molecules by the dialysis process. Additionally, when the suspension pH was increased until 5.5, one degradation step and a residue quantity of around 12% were observed, similar to CNC obtained by other hydrolysis conditions. Moreover, the thermal stability of the CNC obtained with 64 wt% sulphuric acid solution after 30 minutes was similar to CNC isolated using other hydrolysis conditions.

Kim *et al.* [37] studied the carbonization of cellulose by thermogravimetric analysis after immersing cellulose in dilute sulphuric acid for a few minutes. They observed that the pyrolysis of pure cellulose was apparently a one-step reaction, whereas, similar to our results for CNC obtained after 64 wt% sulphuric acid solution for 30 minutes, in sulphuric acid-impregnated cellulose two steps of degradation were observed.

Morphological analysis of CNC is essential in order to understand the effect of different hydrolysis conditions on nanocrystal dimensions. In this way, the dimensions of nanocrystals were measured using AFM microscopy height images. In order to eliminate the effect of tip radius on nanocrystal diameter measurements, it was assumed that CNCs were cylindrical in shape [38]. A minimum of 30 measurements were performed to calculate the average diameter (D) and length (L) of nanocrystals, thus calculating aspect ratio values. AFM height images (Figure 7) revealed that after acid hydrolysis uniform-sized CNCs with

rod-like shape were obtained. Table 4 summarizes the length and diameter values obtained using different acid hydrolysis conditions. The length and diameter values obtained were quite similar, however, the CNCs isolated under 64 wt% sulphuric acid solution for 30 minutes showed slightly higher aspect ratio. In the preparation of bionanocomposites based on CNC, among other parameters, the aspect ratio value of nanocrystals is very important [25]. Siqueira *et al.* [39] reported length and diameter values of 215 ± 67 nm and 5 ± 1.5 nm, respectively, giving an aspect ratio of 43. Instead, the average length and diameter values reported by Garcia de Rodriguez *et al.* [40] were around 250 ± 100 nm and 4 ± 1 nm, respectively, with an aspect ratio around 60. The yield of isolated CNC obtained after the sequence of chemical treatments was about 20% and was determined by weighing.

4 CONCLUSIONS

The main chemical treatments used for the isolation of nanocellulose from sisal fibers were studied. For this purpose, the effect of main chemical reaction conditions in physicochemical and morphological properties of cellulosic samples obtained were evaluated.

Among the different alkali treatment times used, only the cellulosic sample obtained after treating for 240 minutes showed a reduction in the onset and maximum degradation temperature values. Samples treated at 60, 90 and 120 minutes showed similar properties and morphologies, thus the intermediate time was selected for the subsequent chemical treatment.

The sample obtained after acetylation treatment of 30 minutes showed the best thermal stability, however, longer acetylation reaction times of 60 and 90 minutes led to a reduction in the onset temperature values, so the reaction time of 30 minutes was chosen for the next acid hydrolysis treatment.

Concerning acid hydrolysis treatment, all conditions used were adequate to isolate CNC. However, in both sulphuric acid concentrations (32 and 64 wt%), the crystallinity index values decreased when long time reactions were used, suggesting that prolonged hydrolysis times could damage crystal structure. In all samples, the thermal stability of isolated CNC was improved between 20 and 45 °C, increasing suspension pH value from about 3.5 to 5.5 by dialysis process. In addition, the same CNC sample could show one or two degradation steps depending on the pH of the suspension. The CNC with two degradation steps could be associated with cellulose regions with higher amounts of acid molecules.

Finally, it should be noted that nanocellulose with rod-like shape and uniform size were isolated from

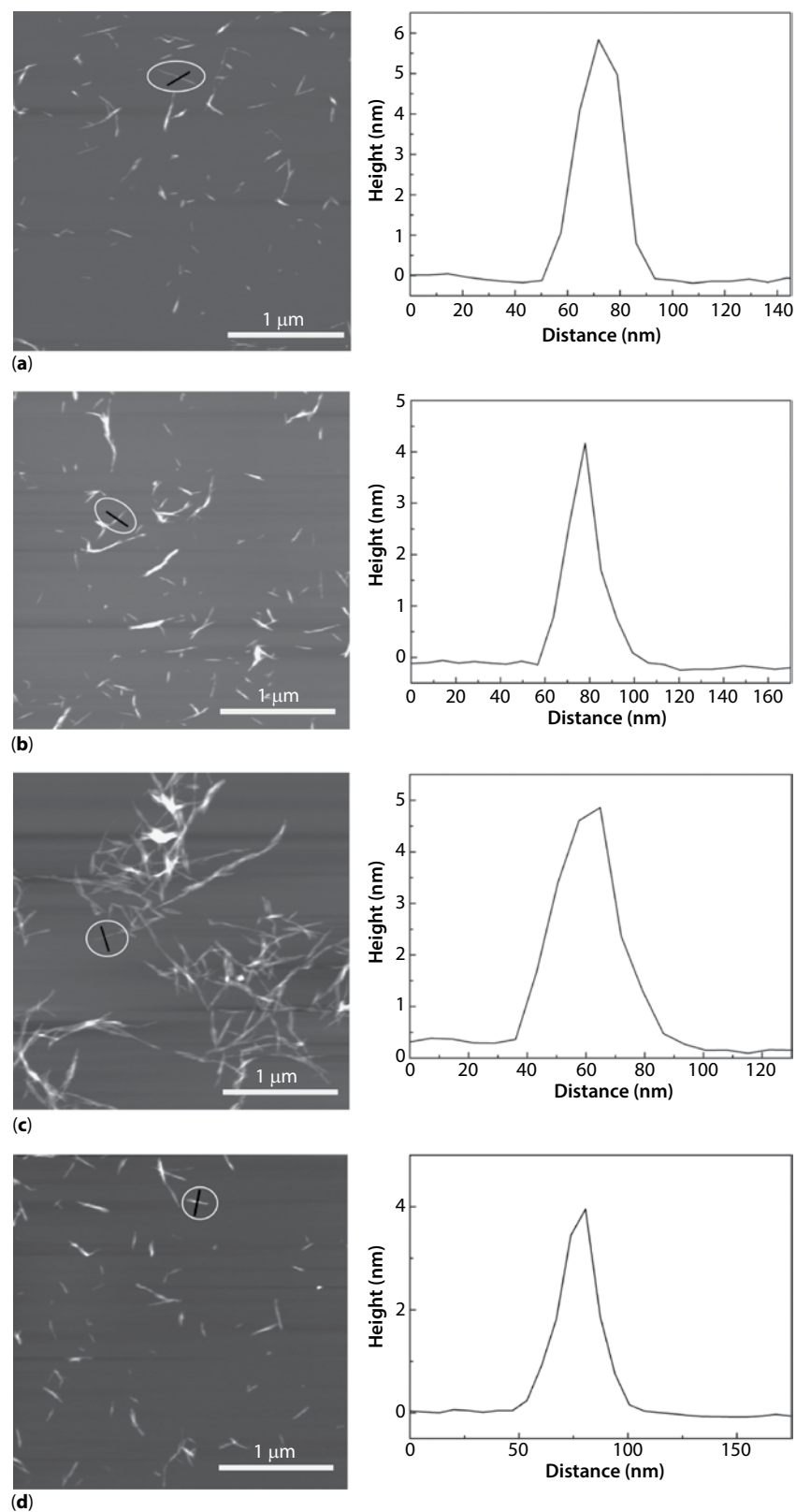


Figure 7 AFM height images and height profiles related to the black lines of sisal cellulose nanocrystals after acid hydrolysis in different concentrations and reaction times: (a) H32-60, (b) H32-120, (c) H64-30 and (d) H64-60.

Table 4 Aspect ratio values of cellulose nanocrystals after acid hydrolysis treatments.

Treatment	Length (nm)	Diameter (nm)	Aspect ratio (L/D)
H32-60	200 ± 37	5 ± 2	40
H32-120	211 ± 50		42
H64-30	224 ± 53		45
H64-60	198 ± 52		40

sisal fibers using a succession of specific chemical treatments, giving an aspect ratio of around 40–45.

ACKNOWLEDGMENTS

The authors are grateful for the financial support from the Basque Country Government in the frame of Consolidated Groups (IT-776-13) and Elkartek 2016 PLAPU3D project. and Spanish Ministry (MAT2013-43076-R). Additionally, G. M. thanks the Basque Government for PhD grant with a reference number BFI-2010-210 (MOD.AE). Technical and human support provided by SGIker Macrobehaviour-Mesostructure-Nanotechnology (UPV/EHU, MINECO, GV/EJ, ERDF and ESF) is also gratefully acknowledged. Finally, we would like to dedicate this manuscript to the distinguished Professor Iñaki Mondragon.

REFERENCES

- M.M.S. Lima and R. Borsali, Rod-like cellulose microcrystal: Structure, properties, and applications. *Macromol. Rapid. Commun.* **25**, 771–787 (2004).
- D. Klemm, B. Heublein, H-P. Fink, and A. Bohn, Cellulose: Fascinating biopolymer and sustainable raw material. *Angew. Chem. Int.* **44**, 3358–3393 (2005).
- J.I. Morán, V.A. Alvarez, V.P. Cyras, and A. Vázquez, Extraction of cellulose and preparation of nanocellulose from sisal fibres. *Cellulose* **15**, 149–159 (2008).
- K. Joseph, R.D.T. Filho, B. James, S. Thomas, and L. Hecker de Carvalho, A review on sisal fiber reinforced polymer composites. *Rev. Bras. Eng. Agr. Amb.* **3**, 367–379 (1999).
- A. Arbelaiz, G. Cantero, B. Fernández, I. Mondragon, P. Gañán, and J.M. Kenny, Flax fibre surface modifications: effects on fibre physico mechanical and flax/polypropylene interface properties. *Polym. Compos.* **26**, 324–332 (2005).
- A. Arbelaiz, B. Fernandez, G. Cantero, R. Llano-Ponte, A. Valea, and I. Mondragon, Mechanical properties of flax fibre/polypropylene composites. Influence of fibre/matrix modification and glass fibre hybridization. *Compos. Part A* **36**, 1637–1644 (2005).
- I. Siró and D. Plackett, Microfibrillated cellulose and new nanocomposite materials: A review. *Cellulose* **17**, 459–494 (2010).
- M.A. Hubbe, O.R. Rojas, L.A. Lucia, and M. Sain, Cellulosic nanocomposites: A review. *Bioresources* **3**, 929–980 (2008).
- G. Mondragon, S. Fernandes, A. Retegi, C. Peña, I. Algar, A. Eceiza, and A. Arbelaiz, A common strategy to extracting cellulose nanoentities from different plants. *Ind. Crop. Prod.* **55**, 140–148 (2014).
- M.A.S.A. Samir, F. Alloin, M. Paillet, and A. Dufresne, Tangling effect in fibrillated cellulose reinforced nanocomposites. *Macromolecules* **37**, 4313–4316 (2004).
- J.F.V. Vincent, From cellulose to cell. *J. Exp. Biol.* **202**, 3263–3268 (1999).
- G. Mondragon, C. Pena-Rodriguez, A. Gonzalez, A. Eceiza, and A. Arbelaiz, Bionanocomposites based on gelatin matrix and nanocellulose. *Eur. Polym. J.* **62**, 1–9 (2015).
- A. Orue, M.A. Corcuera, C. Peña, A. Eceiza, and A. Arbelaiz, Bionanocomposites based on thermoplastic starch and cellulose nanofibers. *J. Thermoplast. Compos. Mater.* DOI: 10.1177/0892705714536424 (2014).
- M. Jonoobi, R. Oladi, Y. Davoudpour, K. Oksman, A. Dufresne, Y. Hamzeh, and R. Davoodi, Different preparation methods and properties of nanostructured cellulose from various natural resources and residues: A review. *Cellulose* **22**, 935–969 (2015).
- L. Brinchi, F. Cotana, E. Fortunati, and J.M. Kenny, Production of nanocrystalline cellulose from lignocellulosic biomass: Technology and applications. *Carbohydr. Polym.* **94**, 154–169 (2013).
- M. Roman and W.T. Winter, Effect of sulfate groups from sulfuric acid hydrolysis on the thermal degradation behavior of bacterial cellulose. *Biomacromolecules* **5**, 1671–1677 (2004).
- L. Segal, J.J. Creely, Jr. A.E. Martin, and C.M. Conrad, An empirical method for estimating the degree of crystallinity of native cellulose using the X-ray diffractometer. *Text. Res. J.* **29**, 786–794 (1959).
- I.M. De Rosa, J.M. Kenny, D. Puglia, C. Santulli, and F. Sarasini, Morphological, thermal and mechanical characterization of okra (*Abelmoschus esculentus*) fibres as potential reinforcement in polymer composites. *Compos. Sci. Technol.* **70**, 116–122 (2010).
- Y. Haiping, Y. Rong, C. Hanping, H.L. Dong, and Z. Chuguang, Characteristics of hemicellulose, cellulose and lignin pyrolysis. *Fuel* **86**, 1781–1788 (2007).
- P. Garside and P. Wyeth, Identification of cellulosic fibres by FTIR spectroscopy: Thread and single fibre analysis by attenuated total reflectance. *Stud. Conserv.* **48**, 269–275 (2003).
- K. Wang, J.X. Jiang, F. Xu, and R.C. Sun, Influence of steaming explosion time on the physico-chemical properties of cellulose from Lespedeza stalks (*Lespedeza crytobotrya*). *Bioresour. Technol.* **100**, 5288–5294 (2009).
- I.M. De Rosa, J.M. Kenny, M. Maniruzzaman, Md. Moniruzzaman, M. Monti, D. Puglia, C. Santulli, and F. Sarasini, Effect of chemical treatments on the mechanical and thermal behaviour of okra (*Abelmoschus esculentus*) fibres. *Compos. Sci. Technol.* **71**, 246–254 (2011).

23. A. Alemdar and M. Sain, Isolation and characterization of nanofibres from agricultural residues – wheat straw and soy hulls. *Bioresour. Technol.* **99**, 1664–1671 (2008).
24. D.N.S. Hon, *Chemical Modification of Lignocellulosic Materials*, Marcel Dekker, New York, USA (1996).
25. N.A. Rosli, I. Ahmad, and I. Abdullah, Isolation and characterization of cellulose nanocrystals from *Agave angustifolia* fibre. *BioResources* **8**, 1893–1908 (2013).
26. A.C.H. Barreto, D.S. Rosa, P.B.A. Fecine, and S.E. Mazzetto, Properties of sisal fibres treated by alkali solution and their application into cardanol-based biocomposites. *Compos. Part A* **42**, 492–500 (2011).
27. A. Arbelaiz, B. Fernández, J.A. Ramos, and I. Mondragon, Thermal and crystallization studies of short flax fibre reinforced polypropylene matrix composites: Effect of treatments. *Thermochim. Acta* **440**, 111–121 (2006).
28. J.X. Sun, X.F. Sun, H. Zhao, and R.C. Sun, Isolation and characterization of cellulose from sugarcane bagasse. *Polym. Degrad. Stabil.* **84**, 331–339 (2004).
29. A. Mandal and D. Chakrabarty, Isolation of nanocellulose from waste sugarcane bagasse (SCB) and its characterization. *Carbohydr. Polym.* **86**, 1291–1299 (2011).
30. W. Chen, H. Yu, Y. Liu, Y. Hai, M. Zhang, and P. Chen, Isolation and characterization of cellulose nanofibers from four plant cellulose fibres using a chemical ultrasonic process. *Cellulose* **18**, 433–442 (2011).
31. N. Wang, E. Ding, and R. Cheng, Preparation and liquid crystalline properties of spherical cellulose nanocrystals. *Langmuir* **24**, 5–8 (2008).
32. L.H. Zaini, M. Jonoobi, Md.T. Paridah, and S Karimi, Isolation and characterization of cellulose whiskers from kenaf (*Hibiscus cannabinus* L.) bast fibres. *J. Biomater. Nanobiotechnol.* **4**, 37–44 (2013).
33. H. Kargarzadeh, I. Ahmad, I. Abdullah, A. Dufresne, S.Y. Zainudin, and R.M. Sheltami, Effects of hydrolysis conditions on the morphology, crystallinity, and thermal stability of cellulose nanocrystals extracted from kenaf bast fibres. *Cellulose* **19**, 855–866 (2012).
34. D. Klemm, B. Philipp, T. Heinze, U. Heinze, and W. Wagenknecht, *Comprehensive Cellulose Chemistry: Fundamentals and Analytical Methods*, Wiley-VCH, Weinheim, Germany (1998).
35. A.C. Corrêa, E.M. Teixeira, L.A. Pessan, and L.H. Capparelli Mattoso, Cellulose nanofibers from curaua fibres. *Cellulose* **17**, 1183–1192 (2010).
36. N. Wang, E. Ding, and R. Cheng, Thermal degradation behaviors of spherical cellulose nanocrystals with sulfate groups. *Polymer* **48**, 3486–3493 (2007).
37. D.-Y. Kim, Y. Nishiyama, M. Wada, and S. Kuga, High-yield carbonization of cellulose by sulfuric acid impregnation. *Cellulose* **8**, 29–33 (2001).
38. I. Kvien, B.S. Tanem, and K. Oksman, Characterization of cellulose whiskers and their nanocomposites by atomic force and electron microscopy. *Biomacromolecules* **6**, 3160–3165 (2005).
39. G. Siqueira, J. Bras, and A. Dufresne, Cellulose whiskers versus microfibrils: Influence of the nature of the nanoparticle and its surface functionalization on the thermal and mechanical properties of nanocomposites. *Biomacromolecules* **10**, 425–432 (2009).
40. N.L. Garcia de Rodriguez, W. Thielemans, and A. Dufresne, Sisal cellulose whiskers reinforced polyvinyl acetate nanocomposites. *Cellulose* **13**, 261–270 (2006).